Available online at www.sciencedirect.com
SCIENCE DIRECT®
International Journal of Mass Spectrometry 239 (2004) 43–49
International Journal of Mass Spectrometry
www.elsevier.com/locate/ijms

An electrostatic focusing ion guide for ion mobility-mass spectrometry

Kent J. Gillig, Brandon T. Ruotolo, Earle G. Stone, David H. Russell*

Laboratory for Biological Mass Spectrometry, Department of Chemistry, Texas A&M University, 3255 TAMU, College Station, TX 77843, USA

Received 26 July 2004; accepted 14 September 2004
Available online 20 October 2004

Abstract

An electrostatic focusing ion guide ion mobility-mass spectrometer (IM-MS) is described. The apparatus consists of a MALDI ion source coupled to an ion drift cell operating at pressures of 1–10 Torr and a small linear time-of-flight (TOF) mass spectrometer. The electrostatic focusing IMS drift cell acts as an ion guide, thus increasing ion transmission while maintaining high resolution. The drift cell is composed of a series of focusing and defocusing electrostatic fields superimposed on the potential drop applied across the drift cell. Calculated ion trajectories for several drift cell configurations, which include Monte Carlo simulations to model ion-neutral collisions, show significantly higher ion transmission and these results are supported by preliminary experimental results. A mobility resolution of ∼100 and detection levels of <10 fmol is demonstrated for peptides ionized by MALDI.

Keywords: Electrostatic focusing ion guide; Ion mobility spectrometry; Mass spectrometry

1. Introduction

Ion mobility spectrometry (IMS) combined with mass spectrometry (MS) is now poised to have a major impact on high-throughput protein identification/characterization, an area of research commonly referred to as proteomics [1]. The IM-MS instrument can be adapted to both electrospray ionization (ESI) [2] and matrix-assisted laser desorption ionization (MALDI) ion sources [3], which are the two most important ionization methods for proteomics research. In addition, several laboratories have introduced new IM-MS instruments that significantly improve sensitivity, resolution, and tandem MS capabilities. The increased experimental versatility and dimensionality of IM-MS relative to MS alone dramatically increases our analytical capabilities with regard to protein identification, thus expanding the frontiers of chemical-biology [4–6].

Separation of ions on the basis of mobility through a buffer gas has been extensively studied [7], and the introduction of atmospheric pressure IMS combined with atmospheric pressure ion sources has opened new avenues for applications in many areas of analytical chemistry [8]. Application of IMS to the detection of explosives continues to be a major area of research and development [9,10], and Hill and coworkers [11] have developed an electrospray ionization (ESI) IMS technique for illicit drug identification and small peptide analysis. IMS has also been particularly useful for studies of carbon and metal containing clusters [12–13b], and more recently a number of laboratories have expanded IMS studies to include problems in biological and polymer chemistry [8b,c]. For example, Bowers coupled MALDI with IM-MS to measure ion collision cross-sections, which can be related to gas-phase conformations of various small peptides and polymer ions, i.e., bradykinin and polyethylene glycol (PEG) [3,14], and Jarrold and coworkers [2,15] used ESI-IM-MS to probe the gas-phase dynamics of protein ions as a function of charge state with the aid of newly developed high resolution IM. Applications of IMS to biomolecules continues to grow and several research groups now use this technique to study folding pathways of anhydrous protein ions [16] and for peptide mass mapping and structural characterization of gas-phase ions of biological importance [17–20]. Recent MALDI-IM-MS studies by Russell and coworkers [19] suggest that IM-

* Corresponding author. Tel.: +1 9798453740; fax: +1 9798459485.
E-mail address: platt@mail.chem.tamu.edu (D.H. Russell).

1387-3806/$ – see front matter © 2004 Elsevier B.V. All rights reserved.
doi:10.1016/j.ijms.2004.09.005

MS methodologies possess increased utility for spectral deconvolution, internal calibration, and peptide identification relative to high resolution MS, and current instrument development efforts in our laboratory focus on issues of resolution, limit of detection, and the analytical utility of IM-MS in terms of peak capacity [21,22].

Although modern IM-MS instruments can achieve impressive resolution [23], sensitivity and limit of detection are typically poor when compared to state-of-the-art mass spectrometers. For example, commercially available MALDI TOF instruments are routinely used to analyze 1–50 fmol amounts of peptides, and under optimum conditions (absence of chemical noise) the analysis of sub-femtomole amounts of peptides can be achieved [24]. The highest reported mobility resolution for single-charged ions is 172 [25], but there are very few examples of femtomole limit-of-detection for biological compounds using an IM apparatus [26]. In addition, high resolution drift cells require high voltages, long drift lengths, and very uniform electric fields, and ion transmission in these drift cells is low due to ion losses by radial diffusion in the drift cell, thus good figures-of-merit in terms of both sensitivity and resolution are difficult to achieve using a single IM-MS instrument arrangement. It is also important to note that high-IM resolution ($t/\Delta t > 50$) is rarely achieved for biological molecules due to conformational broadening effects [27]. For example, Bowers and co-workers utilized well-known transport equations to describe the arrival time distribution (ATD) for an ion population having a single gas-phase conformation to suggest that the peak width for the $[M + H]^+$ ion of bradykinin is broadened due to the presence of multiple, co-eluting gas-phase conformations.

Several factors influence the design of an IM drift cell for applications where both high resolution and high sensitivity are required. If the electric field is uniform along the cell axis but varies as a function of radius, then the ions that diffuse into non-uniform regions will have longer drift times (peak broadening) than ions that remain in the uniform field region [28]. The resolution of a uniform field ion mobility spectrometer is increased by using a high voltage drop, but a high buffer gas pressure must be used to avoid reaching the discharge voltage. Although the use of high pressure and high voltage does not inhibit IMS, the high pressure complicates construction of the IM-MS instrument. That is, high pressure IM-MS requires the use of high capacity vacuum pumps and very small sampling apertures to maintain mass spectrometer vacuum.

In this paper we describe a drift cell design that has higher ion transmission than that of uniform field drift cells. The lens geometry of this drift cell confines the ions near the axis of the cell by using a combination of non-uniform electrostatic fields, which produce periodic electric fields that increase ion transmission but do not degrade resolution [29a]. The ion focusing is accomplished by applying a dc voltage drop across a series of thick aperture electrostatic lenses, creating an applied electric field that is symmetric with respect to the drift axis. As the ions traverse the device they experience nearly identical symmetric electric fields, thus the ions diffuse radially in the uniform field regions and are refocused as they traverse the non-uniform regions. Because the ion motion through the lens system is sinusoidal, the loss of resolution relative to that obtained in a purely uniform electric field is negligible. In principle the device functions as a periodic electrostatic ion guide, i.e., the ions are confined near the drift cell axis, which increases ion transmission by more by more fully illuminating the exit aperture [29b,29c].

2. Experimental

A schematic diagram of the IM-MS apparatus constructed in our laboratory is shown in Fig. 1. The instrument is divided into three main regions: (A) a high pressure MALDI source (1–10 Torr helium), (B) a periodic focusing IM drift cell, and (C) a 20 cm orthogonal time-of-flight mass spectrometer that is positioned perpendicular to the drift cell axis (o-TOF) and coupled to the drift cell by primary ion optics (electrostatic lenses). The TOF ion source and drift cell are mounted on an 8 in.stainless steel flange. Ions exit the drift cell through a small, interchangeable (100–500 μm diameter) aperture. The primary ion optics, mass spectrometer source, and ion mobility detector are housed in a 8 in. stainless steel six-way cross that is pumped by two 550 l/s turbomolecular pumps (Varian model V550). The drift cell can be operated at helium gas pressures of up to 10 Torr, while maintaining the mass spectrometer at an operating pressure of less than 1×10^{-5} Torr. Under these conditions typical drift times for peptide ions of approximately *m/z* 1000 are 1–2 ms, and instrument duty cycles approaching 100% can be achieved by using kHz repetition rate MALDI lasers [30] and specially designed TOF data acquisition hardware and software [31].

The drift cell is contained in a 4 in. outer diameter, 3 in. inner diameter Rulon® tube. The Rulon® material (a ceramic filled Teflon) provides complete electrical insulation yet exhibits low outgassing characteristics. The drift cell consists of twenty-three (23) elements 0.635 cm thick, 6.35 cm outer diameter, 1.50 cm inner diameter stainless steel aperture lenses spaced 0.635 cm apart by 0.794 cm diameter ceramic balls (total drift length 29.5 cm). A non-uniform electric field is established along the drift cell interior by applying a voltage across a resistor chain of 1 MΩ resistors. The maximum voltage that can be applied depends up on the operating pressure of helium. For example, at helium pressure of 1 Torr the maximum voltage that can be applied to the drift cell is approximately 2000 V, e.g., 68 V/cm Torr [32].

The IM source is constructed from a block of Rulon® with the interior milled out to hold the drift cell back plate and first two drift cell aperture discs. The source accessories include a view port, high voltage feedthroughs, buffer gas inlet, pirani gauge, ionization laser port, and sample inlet, all attached with viton o-ring seals and electrically isolated. Ions are formed by irradiating the sample deposited on to a direct insertion probe located midway between the back plate

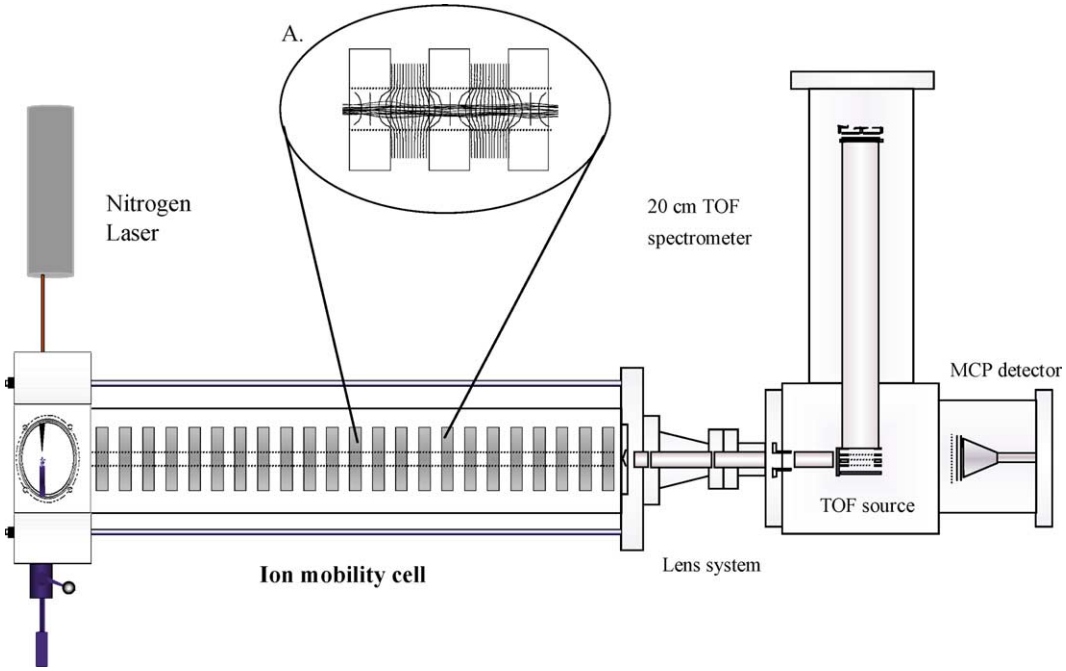

Fig. 1. Schematic diagram of the high-pressure periodic field MALDI/IM-o-TOF apparatus. The inset (A) shows equipotential lines for three aperture lenses and ion trajectory calculations (m/z 720, K_o 4.31, 1 Torr helium) as determined using Simion.

and the first aperture disc with the output from a focused nitrogen laser (Laser Science, 337 nm, 20 Hz) or micro-crystal Nd:YAG (355 nm, variable to 1 kHz) laser at a grazing angle of ∼30° from the drift cell axis.

Ions exiting the drift cell are accelerated and focused by a series of electrostatic lenses into the extraction region of an orthogonal TOF analyzer. Ion mobility spectra are recorded by allowing the ions to pass through the TOF source to an on axis micro-channel plate (MCP) detector. A mass spectrum can be recorded by pulsing the potential applied to the TOF source plates to inject the ions into the o-TOF-MS. The detector signals are recorded using an IonWerks, Inc. (model TDCX4) time-to-digital converter. The mass or mobility spectra are then recorded using real-time data acquisition software (Ionwerks PC card timing controller) with the data displayed as a two-dimensional plot of mobility drift time versus m/z [31].

Ion trajectory calculations, which include the effects of ion/neutral collisions, are modeled as elastic in a non-stationary background gas at 298 K using a modified Simion user program [33–35]. To initiate a simulation, a user-defined initial ion velocity is chosen, the velocity chosen for the results presented here is a MALDI-relevant ion velocity of ∼300–700 m/s, and the Simion user program collision model is called at each time step set shorter than the mean free time between collisions [36]. During the course of a simulation, the program (step 1) calculates the average velocity of the buffer gas using a Maxwell–Boltzmann distribution [37,38]. At a specified neutral gas pressure, the program then (step 2) calculates the mean free time between collisions along with the probability of a collision occurring at each time step [36]. At this point (step 3) a laboratory-frame field-dependant ion velocity (in most cases, this velocity is indicative of a near-thermal average ion velocity) is transformed into the center-of-mass system. During the final portion of a single calculation cycle, the post-collision ion velocity is calculated assuming an isotropic collision (step 4), a random scattering angle is determined (step 5), and the post-collision ion velocity is transformed to the laboratory frame (step 6). This sequence is iterated tens of thousands of times over the course of a typical simulation. For the drift cells simulation results presented here, we evaluated the effects of drift cell length and electrode dimensions (aperture diameter and spacing) on the ion transmission, and the simulations were performed multiple times to add statistical weight to the calculated transmission efficiencies.[1]

3. Results and discussion

The objective of this research is to develop an ion mobility drift cell having high resolution (R = 50–100) and sufficiently high transmission for proteomics applications, i.e., detection limits of fentomoles for peptide ions. In an effort to design an optimum IMS drift cell, we examined a number of systems using computed electrostatic models, including the effects of ion-neutral collisions (Monte Carlo methods). Using these methods we found a combination of electrostatic lens thickness, ratio of aperture diameter and spacing of the lenses that

[1] The SIMION user program discussed in the text is available upon request.

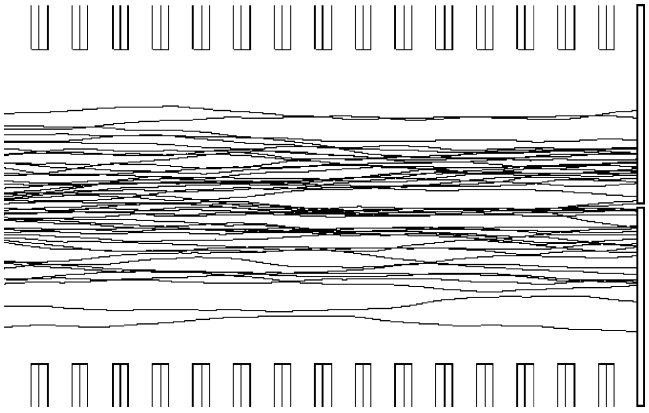

Fig. 2. Plot of ion trajectories (m/z 720, K_o 4.31, 1 Torr helium) at the end of a 100 cm uniform field drift cell.

strongly affect ion transmission. The electrostatic equipotentials defined by thick aperture lenses are shown in the inset (A) of Fig. 1, as well as calculated ion trajectories for $C_{60}^{\bullet+}$ (m/z 720) ions. Note that all ions are confined near the centerline of the drift cell axis, where the electric field varies from approximately 22.5 V/cm within each aperture plate to a maximum of 57.5 V/cm between the aperture plates. That is, the electric field is composed of linear and non-linear elements. Figs. 2 and 3 contain ion trajectory calculations for $C_{60}^{\bullet+}$ ions at a pressure of 1 Torr helium and 30 V/cm applied field for a uniform and non-uniform drift cell, respectively. The figures only show the ion trajectories over last 7.5 cm of a 1 m long drift cells. Note that in the uniform field drift cell (Fig. 2) the transmission of ions through an exit aperture is extremely low ($\sim$1 in 10^3). Although ion transmission can be increased by placing focusing lenses between the drift cell and exit aperture plate, such lenses decrease the drift cell resolution, because ion drift times are dependent on radial positions. In a periodic field (Fig. 3) the ions are confined along the drift cell axis (see inset of Fig. 1), which significantly increases the ion transmission through the exit aperture. The periodic drift cell functions analogously to a segmented quadrupole collision

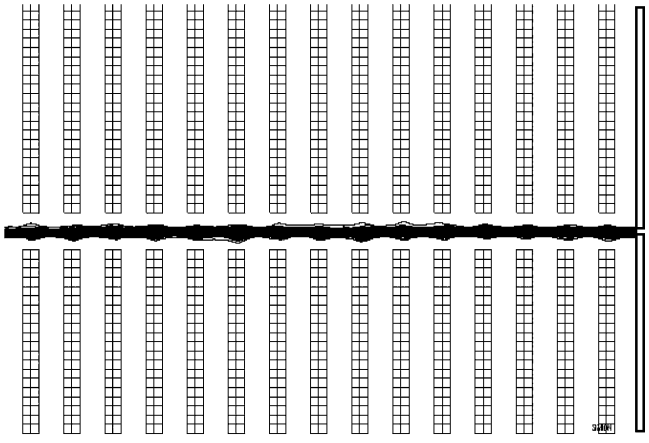

Fig. 3. Plot of ion trajectories (m/z 720, K_o 4.31, 1 Torr helium) at the end of a 100 cm periodic field focusing drift cell.

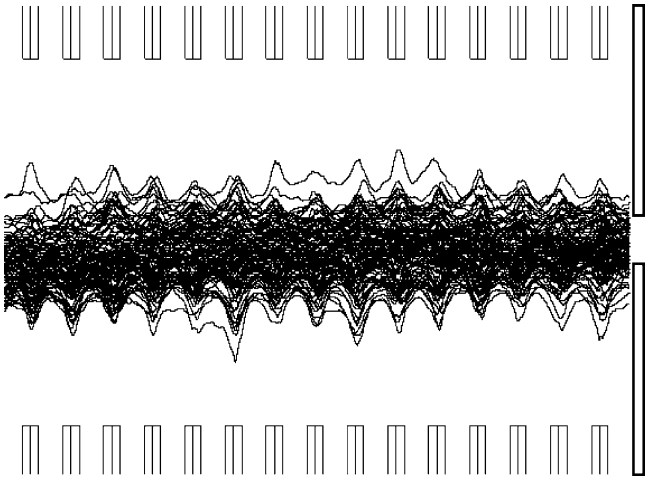

Fig. 4. Ten times radial blowup of ion trajectories shown in Fig. 3.

cell [39]. For example, stabilization of ions and reduction of radial diffusion in the periodic cell occurs by collisional cooling in a static "pseudopotential" in the inertial frame rather than the pseudopotential produced by rf fields in a segmented quadrupole. Fig. 4 shows a 10× radial blowup of the ion trajectories of Fig. 3 illustrating the effects of ion focusing by the non-uniform electrostatic fields. Note also that identical apertures are included in Figs. 2–4 as conceptual tools to indicate the difference in transmission efficiency between a uniform field drift cell and a periodic field drift cell. To compare resolution and percent transmission for a uniform field drift cell versus a periodic field the Monte Carlo simulation was first tested in a uniform field and the results were compared to calculated values from Eqs. (1) and (2). The results obtained using helium buffer gas at a pressure of 1 Torr and field strength of 50 V/cm are shown in Fig. 5. The percent transmission is obtained using Eq. (1).

$$\text{Transmission (\%)} = \left(1 - e^{\frac{-r^2}{4D_L t}}\right) \times 100 \quad (1)$$

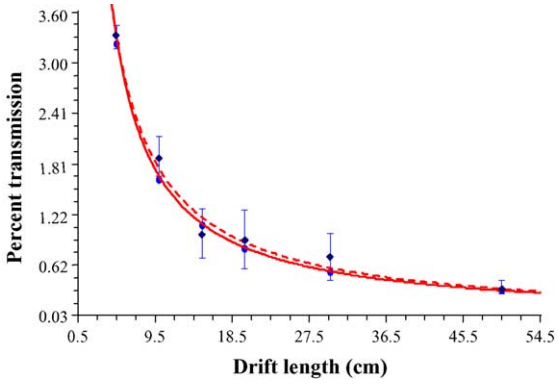

Fig. 5. Plot of percent transmission vs. drift cell length for a uniform field cell. Calculations using the Simion Monte Carlo method (filled diamonds, 10,000 trajectories averaged per data point, 1 Torr helium) and Wannier's equation (filled circles) including best fits (dashed line and solid line, respectively).

where r is the aperture radius, t is time, and D_t is the transverse diffusion. The transverse diffusion is calculated using Wannier's radial diffusion term

$$D_t = \frac{k_b T}{q} K + \frac{m}{3} \times \frac{m+M}{m+1.908M} \times \frac{E^2 K^3}{q} \quad (2)$$

where k_b is the Boltzman constant, T is the temperature, K is the mobility, m is the mass of the neutral drift gas, q is the ion charge, M is the mass of the ion mass, and E is the electric field strength [40]. The theoretical values of percent transmission for a uniform field at 1 Torr through a 500 μm aperture are shown in Fig. 5. These values are close to that obtained by Monte Carlo simulation (~5% error), which suggest a realistic simulation of ion/neutral hard sphere collisions for any electric field arrangement over a large E/N range is possible with this model. The simulation was then performed for a number of periodic drift cells with different electrode dimensions (i.e., electrode thickness, diameter, and spacing). Fig. 6 shows plots of the increase in percent transmission versus drift cell length for four drift cells having different electrode dimensions. Because the data shown in Fig. 6 is derived from simulations similar to those shown in Fig. 5, the errors in the reported increase in percent transmission are also similar. Consequently, data points for Fig. 6 exhibit an average standard deviation of ±5% transmission. Periodic field 1 refers to a drift cell consisting of 4 mm thick electrodes spaced 4 mm apart with 4 mm diameter lens apertures, periodic field 2 refers to a drift cell consisting of 6 mm thick electrodes spaced 6 mm apart with 6 mm diameter lens apertures, periodic field 3 is identical to periodic field 2 but the diameter lens aperture was increased to 1 cm, and periodic field 4 is identical to periodic field 2 but the diameter of the lens apertures is 1.5 cm. The increase in percent transmission for a periodic field drift cell versus a uniform field drift cell, under otherwise identical conditions, ranges from ~5 to 65 at a 50 cm cell length depending on the electrode configuration. Thus, the simulations indicate that a 50 cm uniform field drift cell would have a transmission of 0.3%, as compared to approximately 20% for an optimized periodic field drift cell.

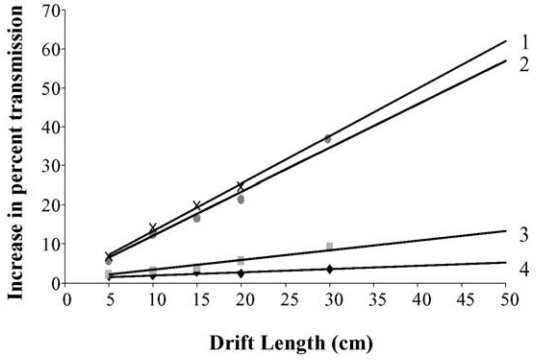

Fig. 6. Calculated increase in percent ion transmissions from Monte Carlo ion/neutral collision simulations for four different drift cells at 1 Torr helium. As referred to in the text: periodic field 1, X; periodic field 2, gray filled circle; periodic field 3, gray filled square; and periodic field 4, black filled diamond.

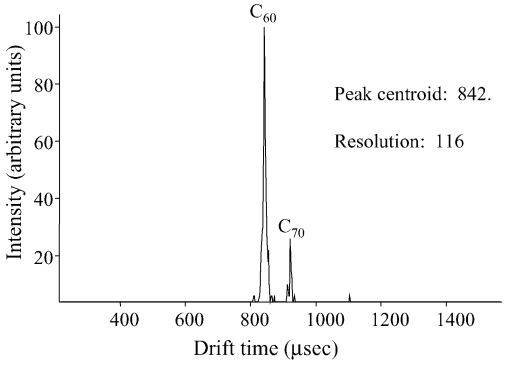

Fig. 7. Ion mobility spectrum of laser desorbed C_{60} and C_{70} demonstrating high-resolution capability.

Note that simulation data was acquired for drift cells having a maximum length of 30 cm, and predicted transmission values for longer drift cells are derived from linear fits to the existing simulation data. Our calculations predict that the optimal drift cell configuration for ion transport at 1 Torr is cell #1, which has electrodes with inner diameter, thickness, and spacing of equal dimensions (periodic fields 1 and 2). The increase in percent transmission is proportional to the inner diameter, the smaller the diameter the greater the increase.

Proof-of-concept experiments were performed to test the results of the Monte Carlo simulations in terms of resolution and ion transmission. Fig. 7 shows an ion mobility spectrum of laser desorbed $C_{60}^{\bullet+}$ and $C_{70}^{\bullet+}$ recorded by the mobility detector (see Fig. 1). In these experiments we used a 29.5 cm periodic cell at a helium pressure of approximately 4 Torr and an applied potential of 1400 V (~12 V/cm Torr), and a mobility resolution ($t/\Delta t$, measured at FWHM) for $C_{60}^{\bullet+}$ ion signals is approximately 120. This resolution is significantly greater (approaching two fold) than the predicted resolution of 70 for a uniform field ion mobility spectrometer operated with the same voltage [41]. Although a resolution of 120 for a low-pressure drift cell meets our design objectives, we also evaluated the performance of the device using biological samples. Fig. 8 shows a similar drift time distribution for the $[M+H]^+$ ions of a model peptide (Gramicidin S) obtained

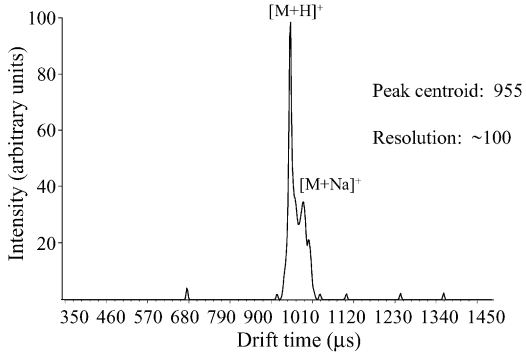

Fig. 8. Drift time distribution of Gramicidin S demonstrating high-resolution capability for biological molecules.

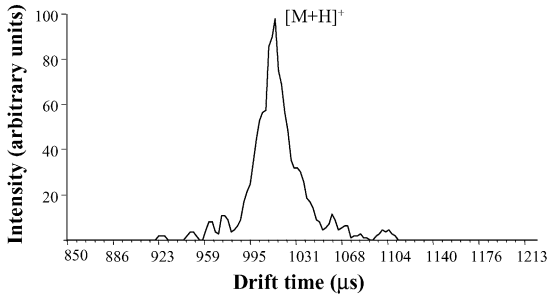

Fig. 9. Drift time distribution of 6 fmol of α-melanocyte stimulating hormone (MW 1665) deposited. The data was accumulated over a 1-min acquisition period, a total of 1200 laser shots.

using a 45 cm periodic drift cell. Note, that the data shown in Fig. 8 are detected using the TOF detector, thus the signals are mass analyzed as the ions elute the mobility drift tube. Ions in this case were formed by MALDI at near threshold laser power and 2390 V (53 V/cm Torr) was applied to the drift cell. Note that both $[M + H]^+$ *m*/*z* 1141.5 and $[M + Na]^+$ *m*/*z* 1163.5 ions are separated and the resolution (FWHM) is approximately 100.

To test the ion transmission through the 29.5 cm periodic spectrometer, a limit of detection experiment was performed. Six femtomoles of α-melanocyte stimulating hormone (MW 1665) was co-deposited with α-cyano-4-hydroxycinnamic acid as a matrix on a probe tip and laser desorbed by 337 nm radiation near threshold in the spectrometer source. The 337 nm nitrogen laser was operated at 20 Hz and mass spectra were accumulated for 1 min over a range of ion mobility arrival times from 0.5 to 1.5 ms. The resulting drift time distribution recorded on the orthogonal time-of-flight detector is shown in Fig. 9. This limit of detection measurement has been repeated and improved upon using a higher beam quality, high repetition rate laser [30]. Limit of detection experiments were also attempted with a 30 cm uniform field spectrometer operating under the same conditions (6 fmol loadings of α-melanocyte stimulating hormone) but no detectable signal was obtained. Using the uniform field device, signal was only obtained by using very high (picomole) sample loadings.

4. Conclusions

There are few analytical methods available to accommodate the high-throughput and high sensitivity requirements of proteomic research. The novel periodic focusing ion drift cell presented here exhibits both excellent resolution and sensitivity in comparison to current high-resolution ion mobility spectrometers. A resolution of 120 clearly demonstrates the high performance characteristics of the periodic focusing drift cell. The reason(s) for the increased resolution over that of a uniform field is unclear, but we are continuing to investigate various parameters that affect resolution [42]. In addition, operating at low pressure circumvents problems associated with sampling of ions from a high-pressure environment. Longer optimized periodic drift cells are being constructed to increase the resolution further without sacrificing sensitivity, thereby aiding the analysis of complex, digested mixtures of proteins [19].

Acknowledgements

The authors gratefully acknowledge Katrin Fuhrer and Valerie Raznikov for help with Monte Carlo simulations. This work was supported by grants from the National Science Foundation (DBI 0116685**)** and U.S. Department of Energy, Division of Chemical Sciences, BES (DE-F602-04ER15520).

References

[1] W.P. Blackstock, M.P. Weir, Tibtech. 17 (1999) 121.
[2] D.E. Clemmer, R.R. Hudgins, M.F. Jarrold, J. Am. Chem. Soc. 117 (1995) 10141.
[3] G. von Helden, T. Wyttenbach, M.T. Bowers, Int. J. Mass Spectrom. Ion Process. 146/147 (1995) 349.
[4] E.G. Stone, K.J. Gillig, B.T. Ruotolo, K. Fuhrer, M. Gonin, A. Schultz, D.H. Russell, Anal. Chem. 73 (2001) 2233.
[5] E.G. Stone, K.J. Gillig, B.T. Ruotolo, D.H. Russell, Int. J. Mass Spectrom. 212 (2001) 519.
[6] C.S. Hoaglund-Hyzer, J. Li, D.E. Clemmer, Anal. Chem. 72 (2000) 2737.
[7] E.A. Mason, E.W. McDaniel, The Mobility and Diffusion of Ions in Gases, John Wiley & Sons Inc., New York, 1973.
[8] (a) T.W. Carr (Ed.), Plasma Chromatography, Plenum Press, New York, 1984;
(b) T. Wyttenbach, M.T. Bowers, Top. Curr. Chem. 225 (2003) 207;
(c) E.S. Baker, J. Gidden, D.P. Fee, P.R. Kemper, S. Anderson, M.T. Bowers, Int. J. Mass Spectrom. 227 (2003) 205.
[9] R.G. Ewing, D.A. Atkinson, G.A. Eiceman, G.J. Ewing, Talanta 54 (2001) 515.
[10] G.A. Eiceman, Z. Karpas, Ion Mobility Spectrometry, CRC Press, Boca Raton, 1994.
[11] (a) L.M. Matz, H.H. Hill, Anal. Chem. 73 (2001) 1664;
(b) G.R. Asbury, H.H. Hill Jr., Anal. Chem. 72 (2000) 580.
[12] P. Dugourd, R.R. Hudgins, A.A. Shvartsburg, M.F. Jarrold, Theory At. Mol. Clusters (1999) 347.
[13] (a) D.E. Clemmer, M.F. Jarrold, J. Mass Spectrom. 32 (1997) 577;
(b) M.T. Bowers, P.R. Kemper, G. von Helden, P.A.M. van Koppen, Science 260 (1993) 1446.
[14] G. von Helden, T. Wyttenbach, M.T. Bowers, Science 267 (1995) 1483.
[15] K.B. Shelimov, M.F. Jarrold, J. Am. Chem. Soc. 119 (1997) 2987.
[16] (a) C.S. Hoaglund-Hyzer, A.E. Counterman, D.E. Clemmer, Chem. Rev. 99 (1999) 3037;
(b) M.F. Jarrold, Acc. Chem. Res. 32 (1999) 360.
[17] K.J. Gillig, B.T. Ruotolo, E.G. Stone, D.H. Russell, K. Fuhrer, A.J. Marc Gonin, Schultz, Anal. Chem. 72 (2000) 3965.
[18] K.B. Shelimov, D.E. Clemmer, R.R. Hudgins, M.F. Jarrold, J. Am. Chem. Soc. 119 (1997) 2240.
[19] B.T. Ruotolo, K.J. Gillig, E.G. Stone, K. Fuhrer, M. Gonin, J.A. Schultz, D.H. Russell, Int. J. Mass Spectrom. 219 (2002) 253.
[20] J. Gidden, M.T. Bowers, J. Phys. Chem. B 107 (2003) 12829–12837.
[21] B.T. Ruotolo, G.F. Verbeck, L.M. Thomson, K.J. Gillig, D.H. Russell, J. Am. Chem. Soc. 124 (2002) 4214.

[22] B.T. Ruotolo, K.J. Gillig, E.G. Stone, D.H. Russell, J. Chrom. B 782 (2002) 385.
[23] G.R. Asbury, H.H. Hill, J. Microcolumn Sep. 12 (2000) 172.
[24] F.H. Strobel, T. Solouki, M.A. White, D.H. Russell, J. Am. Soc. Mass Spectrom. 2 (1991) 91.
[25] P. Dugourd, R.R. Hudgins, D.E. Clemmer, M.F. Jarrold, Rev. Sci. Instrum. 68 (1997) 1122.
[26] C.S. Hoaglund-Hyzer, Y.J. Lee, A.E. Counterman, D.E. Clemmer, Anal. Chem. 74 (2002) 992.
[27] C. Wu, W.F. Siems, J. Klasmeier, H.H. Hill, Anal. Chem. 72 (2000) 391.
[28] W.F. Siems, C. Wu, E.E. Tarver, H.H. Hill, P.R. Larsen, D.G. McMinn, Anal. Chem. 6 (1994) 4195.
[29] (a) K.J. Gillig, D.H. Russell, US Patent 6,639,213;
(b) G. Shenheng, A.G. Marshall, J. Am. Soc. Mass Spectrom. 7 (1996) 101;
(c) A. Septier (Ed.), Focusing of Charged Particles, Academic Press, New York, 1967.
[30] J.A. McLean, D.H. Russell, J. Proteome Res. 2 (2003) 428.
[31] K. Fuhrer, M. Gonin, M.I. McCully, T. Egan, S.R. Ulrich, V.W. Vaughn, W.D. Burton Jr., J.A. Schultz, K.J. Gillig, D.H. Russell, Proceedings of the 49th Conference of the American Society for Mass Spectrometry, May 27–29, Chicago, IL, 2001.
[32] J.M. Meek, J.D. Craigs, Electrical Breakdown of Gases, Wiley, Chichester, New York, 1978.
[33] L. Ding, M. Sudakov, S. Kumashiro, Int. J. Mass Spectrom. 221 (2002) 117.
[34] A.D. Appelhans, D.A. Dahl, Int. J. Mass Spectrom. 216 (2002) 269.
[35] L. He, D.M. Lubman, Rapid Comm. Mass Spectrom. 11 (1997) 1467.
[36] P.L. Houston, Chemical Kinetics and Reaction Dynamics, McGraw-Hill, New York, 2001.
[37] V.V. Raznikov, I.V. Soulimenkov, V.I. Kozlovski, A.R. Pikhtelev, M.O. Raznikova, T. Horwath, A.A. Kholomeev, Z. Zhou, H. Wollnik, A.F. Dodonov, Rapid Commun. Mass Spectrom. 15 (2001) 1912.
[38] V.V. Raznikov, A.F. Dodonov, M.O. Raznikova, T. Horvath, N. Nankov, H. Wollnik, Adv. Mass Spectrom. 15 (2001) 421.
[39] G. Javahery, B.J. Thompson, J. Am. Soc. Mass Spectrom. 8 (1997) 697.
[40] P.R. Kemper, M.T. Bowers, J. Am. Soc. Mass Spectrom. 1 (1990) 197.
[41] P. Watts, A. Wilder, Int. J. Mass Spectrom. Ion Process. 112 (1992) 179.
[42] G. F. Verbeck, B. T. Ruotolo, K. J. Gillig, D. H. Russell, J. Am. Soc. Mass Spectrom (in press).